



Emissions analyses of humidified cracked ammonia swirling flames

Jordan Davies^{a,*}, Syed Mashruk^a, Daisuke Sato^{a,b}, Luca Mazzotta^c, Daniel Pugh^a, Agustin Valera-Medina^a

^a College of Physical Sciences and Engineering, Cardiff University, Wales CF24 3AA, UK

^b Department of Mechanical Engineering, Kyoto University, Kyoto daigaku-Katsura, Nishikyo-ku, Kyoto 615-8540, Japan

^c Sapienza University of Rome, Via Eudossiana 18, 00133 Rome, Italy

ARTICLE INFO

Keywords:

Ammonia
Hydrogen
Combustion
Humidification
Emissions

ABSTRACT

Using renewably produced ammonia as a zero-carbon fuel is gaining momentum due to its ease of transportation and storage as a hydrogen vector. This is particularly true for partially cracking ammonia immediately prior to use, injecting a blend of NH₃, H₂ and N₂. Challenges with this fuel combination relate to the emissions of NO_x and unburned NH₃, as well as understanding flame stability for practical applications. In this study, a 20 %_(vol.) cracked ammonia blend was investigated using a fully premixed swirl burner, operating at a thermal power of 10 kW with steam injection of 30 %_(vol.) of the fuel and preheating inlet temperatures of up to 390 K, for a range of equivalence ratios from lean to rich. Emissions of NO, NO₂, N₂O, NH₃, H₂, O₂ and H₂O were recorded, along with OH*, NH* and NH₂* chemiluminescence. Additionally, a numerical investigation was conducted using CHEMKIN-PRO to elucidate the main reactions responsible for reducing emissions by providing a rate of production analysis. The 20 %_(vol.) cracked ammonia blend was found to reduce NO, NO₂ and N₂O significantly, with an increase in NH₃ emissions at rich conditions and instabilities at both lean and rich extremes, compared to the widely investigated 70/30_(vol. %) ammonia/hydrogen blend. Humidification reduced NO and NO₂ emissions due to a reduction in HNO production via OH and NH but caused an increase in N₂O by reducing the flame temperature and unburned NH₃ emissions at rich, low power conditions due to combustion instabilities. Unburned H₂ emissions however were reduced, likely relating to a reduction in exhaust temperature thermally cracking less unburned NH₃ into H₂ and N₂.

1. Introduction

Green ammonia is gaining traction as a zero-carbon fuel for combustion in gas turbines, industrial burners and internal combustion engines as it is an effective and low-cost hydrogen carrier [1].

Low reactivity, emissions of NO_x and unburned NH₃, and flame stability are the main challenges relating to the direct use of pure ammonia in large scale combustion systems. Research on ammonia as a fuel has increased rapidly in recent years [2,3] and has demonstrated the high ignition temperature and delay times [4], low flame speed [5] and associated narrow stability limits [6,7] can all be improved by blending ammonia with hydrogen. This is convenient because ammonia contains hydrogen, some of which can be separated out immediately prior to combustion through a partial cracking process at relatively low temperatures [8], possibly using waste heat from the combustor. A recent review on cracking [9] discussed a high-entropy alloy

cobalt-molybdenum catalyst which could achieve the 20 % NH₃ cracking required here at 350°C. This catalyst was also significantly less expensive than conventional ruthenium-based catalysts. The review discussed iron-based catalysts which are even more affordable but need higher temperatures of >600°C. Although blends of ammonia and hydrogen have been shown to have better fundamental combustion performance, NO_x emissions remain problematic unless operating at rich equivalence ratios which emit unburned ammonia [10,11]. Therefore, a significant body of research on limiting NO_x emissions from ammonia/hydrogen flames has grown in recent years. Such experimental works include pressurisation, staging, stratification and humidification.

Pugh et al. [12] showed pressurisation of an NH₃/H₂ flame at an equivalence ratio of $\Phi = 1.2$ up to 0.185 MPa reduced NO_x by nearly an order of magnitude to less than 100ppmvd (15 % O₂). It was noted that increasing pressure also resulted in an increase in unburned NH₃ due to instabilities. In another study [13], they found at lean conditions

* Corresponding author.

E-mail address: Daviesj129@cardiff.ac.uk (J. Davies).

<https://doi.org/10.1016/j.combustflame.2025.113984>

Received 7 June 2024; Received in revised form 9 January 2025; Accepted 13 January 2025

Available online 19 January 2025

0010-2180/© 2025 The Author(s). Published by Elsevier Inc. on behalf of The Combustion Institute. This is an open access article under the CC BY license (<http://creativecommons.org/licenses/by/4.0/>).

pressurisation also reduced N_2O emissions from an enhancement of third body consumption, although significant NO emissions remained at this condition. Similar results were found for NO at lean conditions in [14] but it was noted that as equivalence ratio was reduced, the effect of pressure reducing NO became marginal. Although this study identified pressurised lean flames as a viable option for low NO , it did not measure N_2O emissions, which are known to increase as equivalence ratio is reduced, as presented in [13,15]. Furthermore, it must be noted that increasing pressure does not seem to have a great impact after a certain pressure value, as shown by Ditaranto et al. [15], who additionally demonstrated that NO_x emissions flatten above pressures between 4 and 6 bar. On air staging in pure ammonia flames, Pugh et al. [16] demonstrated that while secondary air loading could provide favourable emissions, it could also cause an increase in NO and NO_2 emissions if not carefully controlled. Elbaz et al. [5] concluded that staging would likely require extensive retrofitting, suggesting single stage concepts would be more viable in the short term. Mashruk et al. [17] reported that stratifying the fuel streams by taking H_2 from the outer premixed flame and injecting it centrally as a diffusion flame reduced NO emissions by roughly 75 % at $\Phi = 0.8$ when operating at 100 % H_2 stratification.

Another, long-established method for reducing emissions from conventional fossil fuels is steam injection. Steam injection has been known to reduce NO_x emissions and increase cycle efficiency in gas turbines operating on natural gas [18–20] and blends of methane and hydrogen [21]. There had been limited research on this effect in ammonia-based fuels until recently. Research by Pugh et al. on steam injection into NH_3/H_2 flames showed reduced NO and increased N_2O but noted water loading above 56 % steam/fuel mass ratios caused blowoff [12,13]. Gutesa et al. [22] showed similar humidification ratios, finding out that NH_3/H_2 flames could withstand up to 72 % steam/fuel mass ratio before blowoff occurred. This is an expected outcome as humidification has been shown to reduce laminar burning velocity in ammonia flames, reducing flame stability [23].

Knowledge of ammonia corrosion and degradation is important for practical application of ammonia combustion. Ammonia causes corrosion when exposed to metals such as copper, zinc, aluminium, and their alloys, so steel has been used for ammonia storage. However, ammonia contaminated by air increases the chances of stress corrosion cracking of steel, especially if it contains nickel or molybdenum [24,25]. To eliminate this condition, the addition of water in the range of 0.08 % to 0.5 % by weight has been shown to mitigate the effect of oxygen and act as an inhibitor of corrosion cracking of steel [26]. Recent studies [27,28] have proposed the use of Inconel alloys for ammonia combustion and studied the impact of hydrogen embrittlement and nitration, although the detailed material science involved is still insufficient. Additionally, water vapor in the combustion exhaust gases is damaging to gas turbine blades. Research by Chen et al. [29] has shown that increased water vapor levels have a significant negative impact on the long-term durability of hot section components such as substrate blades, oxidation resistant coatings, thermal barrier coatings (TBCs), and environmental barrier coatings (EBCs). However, these issues need to be solved to facilitate combustion of any hydrogen-based fuel, which emit significantly more water vapour than an equivalent fossil fuel. The increase in water vapour in the exhaust from a small amount of steam injection to mitigate NO_x emissions would be relatively small compared to the general conversion from fossil fuel to hydrogen-based fuels so would likely be compatible with new materials developed for zero-emission combustion without significant additional research requirements.

It should be noted that the partial cracking of ammonia results in the production of both hydrogen and nitrogen, which few of the above studies included. While the nitrogen can be removed using a molecular sieve, this adds cost and complexity to the combustion system. Therefore, the present work analyses the effect on emissions from keeping nitrogen in the fuel mixture. It also presents the first findings on emissions of NO , NO_2 , N_2O and NH_3 from humidified ammonia/hydrogen/nitrogen flames. This is important as industrial applications of

ammonia/hydrogen flames are likely to include the nitrogen fraction from the cracking process. Further novelty and relevance to industrial applications came from utilising an integrated system to raise steam using waste heat from the combustor, rather than using separate electric heaters.

2. Experimental and numerical setup

2.1. Swirl burner

The optically accessible burner shown in Fig. 1 was operated at a constant thermal power of 10 kW for all conditions. An atmospheric blend of 70/30 %_(vol.) NH_3/H_2 was compared to 20 %_(vol.) cracked ammonia (66.7/25/8.3 %_(vol.) $\text{NH}_3/\text{H}_2/\text{N}_2$) for equivalence ratios $0.6 < \Phi < 1.4$. For industrial applications it is practical and cost effective to store only one fuel in the form of ammonia, then crack the hydrogen required to improve combustion characteristics immediately prior to combustion. However, the cracking process also produces nitrogen. Therefore, the effect on emissions from injecting this nitrogen into the flame as part of the fuel blend was investigated. As the ammonia cracking process produces three hydrogen molecules for each nitrogen molecule, 20 %_(vol.) cracked ammonia was selected for comparison with 70/30 %_(vol.) NH_3/H_2 as it gives a ratio of NH_3 to H_2 near to 70/30 %_(vol.) as well as the required $\text{H}_2:\text{N}_2$ ratio of 3:1. The effects of preheating the air and fuel to 390 K and injecting steam at a ratio of 30 %_(vol.) of the fuel were then examined. 390 K was selected to ensure steam injected into the mixing chamber was maintained in the vapour phase.

Fuel and air were supplied using Bronkhorst thermal mass flow controllers (± 0.5 % between 15 and 95 % of maximum flow) while liquid water was supplied using a Bronkhorst Coriolis mass flow controller. Water was boiled using waste heat from the burner and injected as steam into the plenum to mix with the preheated air and fuel. This mixture then flowed through the injector nozzle ($d = 31.5$ mm) via a radial-tangential swirler ($S_g = 1.05$), using a central injection lance ($d = 22.5$ mm) as a bluff body. The hydrogen was injected at the base of the swirler and mixed with the preheated air, fuel and steam as in [30]. The flame was confined within a quartz glass tube ($d = 156$ mm) to maintain optical access for chemiluminescence imaging and spectroscopy. The flame was monitored using a Logitech Brio camera from a distance of 5 m.

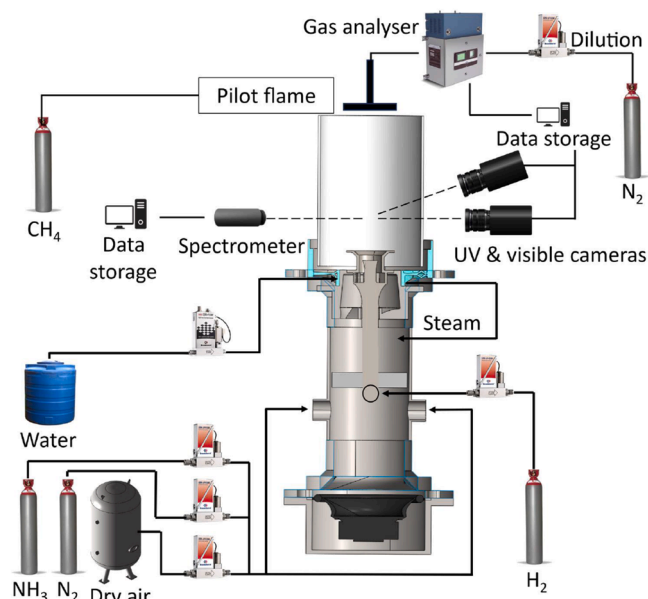


Fig. 1. Simplified schematic of experimental setup (not to scale).

2.2. Exhaust gas and temperature measurements

An Emerson CT5100 quantum cascade laser gas analysis system was used to measure NO, NO₂, N₂O, NH₃, O₂ and H₂O simultaneously at a temperature of 463 K and sampling rate of 1 Hz ($\pm 1\%$ repeatability, 0.999 linearity). For all emissions, 120 samples were averaged over a two-minute period. When raw readings were above the analyser's range, N₂ was used to dilute the sample back into range ($\pm 10\%$ repeatability) as explained in [30]. As the gas analysis system features independent detectors, it was possible to record and present the concentration of other pollutants which remained within range, undiluted and hence with improved uncertainty. Samples were collected from a sampling cross spanning the entire quartz confinement 25 mm above its exit and carried along a heated line to the analyser. Measured oxygen content was negligible with a stoichiometric flame, demonstrating no outside air was entrained into the sampling cross. Samples were captured wet and normalised to dry 15 % O₂ following (equation (10) in [31]). Ongoing discussion surrounds this emissions normalisation method due to the penalty against hydrogen-based fuels stemming from their increased water content in the exhaust gas, compared to carbon-based fuels. When this water content is removed to present dry emission values, the pollutants in the remaining mixture are more concentrated, increasing the apparent emissions on a dry, 15 % O₂ ppmv basis. A suggested alternative is to present emissions on a mass/power basis, e.g. mass of NO emitted per unit of thermal power [32]. Although the present study does not compare between hydrogen and carbon-based fuels, it does include both nitrogen and steam injection, which could dilute the exhaust gas sample and suggest that emissions were lower on a volumetric basis. To account for this dilution and enable a more representative comparison, emissions were also normalised on a mass/power basis, following the methodology presented by Douglas et al. [32].

A mixture of R and K-type thermocouples were used to control inlet temperature, determine temperatures within the combustion chamber and to estimate heat loss for informing chemical reactor network simulations. All temperature measurements were sampled at a rate of 1 Hz and averaged over 120 readings. An R-type thermocouple was positioned centrally in the combustion chamber, located in a fixed position 50 mm upstream of the chamber outlet to determine variations in post-flame zone temperatures across different conditions and was corrected for radiative and convective heat losses.

2.3. Chemiluminescence measurements

Time averaged images of the flame were recorded for OH* (309 nm; A²Σ⁺-X²Π system) with a 310 nm bandpass filter (10 nm FWHM), NH* (336 nm; A³Π-X²Σ system) with a 337 nm bandpass filter (10 nm FWHM) and NH₂* (630 nm; single peak of NH₂ α band) with a 632 nm bandpass filter (10 nm FWHM) by two LaVision cameras each with a Sony ICX285AL sensor and Hamamatsu HB1058 intensifier). These cameras were triggered simultaneously at a sampling rate of 10 Hz for a period of 20 s. After subtracting the background and conducting a 3 × 3 pixel median filter, the images were averaged in Davis v10. Finally, the averaged images went through an Abel Deconvolution Matlab script [33] and were then normalised either to their own or the group maximum. To aid in quantitatively assessing variations in flame morphology between operating conditions, a Matlab script for calculating the intensity weighted centroids of each flame image was written. This calculation accounted for both the distribution of pixels and their relative intensity.

The broad-band nature of the NH₂* [34] and H₂O* [35] which make up the visible range chemiluminescent signature in ammonia-fuelled flames has called into question the validity of using measurements of the NH₂* intensity as an indicator of ground state NH₂ concentration. The authors could not find any studies comparing NH₂ chemiluminescence and ground state NH₂ utilising PLIF. However, a recent study from Konnov [36] suggested that H₂O* was only significant

in the near UV range, NO₂* intensity peaked below an equivalence ratio of 0.8 and that NO₂* intensity decreased as ammonia content increased. Another study from Weng et al. [37] agreed that at lean conditions, the visible chemiluminescence signature could be attributed to NO₂*, but only in the post-flame zone. In the flame zone, the signature was almost exclusively NH₂* at all equivalence ratios. Owing to the high ammonia content in the flames presented here, the relatively rich equivalence ratios of at least 0.8 and the chemiluminescence images being mainly of the flame zone, it was deemed appropriate to assume a positive correlation between the excited NH₂* intensity and ground state NH₂ concentration.

A collimating lens for UV/visible light was mounted 30 mm above the burner outlet and 240 mm away from the central axis. Via a 600 μm fiber optic cable, it was connected to an Avaspec-ULS4096CL spectrometer with a 100 μm slit and 300 lines/mm grating, resulting in a 4.6 nm (FWHM) resolution. The spectrometer featured a 4096-pixel CMOS detector measuring 7 × 200 μm, which was set to an exposure time of 1 s and averaged over 20 scans to improve signal to noise ratio. Background scans were captured prior to flame ignition and subtracted from each datapoint. OH*, NH* and NH₂* intensities taken from the same ranges as the chemiluminescent images discussed above were captured and normalised to each species' maximum.

2.4. Chemical reactor network

To understand the most significant chemical reactions in the formation of emissions, one-dimensional numerical simulations of the flame were carried out using CHEMKIN-PRO. Five inlets for air, NH₃, H₂, N₂ and H₂O were used with four perfectly stirred reactors (PSR) modelling the pre-mixing, flame, central recirculation zone (CRZ) and external recirculation zone (ERZ). To simulate the reactions in the post-flame zone, the outlet of the flame zone PSR fed into a plug flow reactor (PFR). A diagram of the Chemical Reactor Network (CRN) is shown in Fig. 2 and further details including determination of recirculation strength can be found in [11,30,38]. As the same burner geometry was used with similar fuel blends, equivalence ratios and thermal powers as the previous study, the same CRN was deemed an appropriate starting point. To evaluate the contribution of different reactions in the production and consumption of NO and N₂O, absolute rate of production (ROP) values were used in the flame zone, and integrated values of production were used in the post flame zone. Initial heat loss values were estimated from thermocouple measurements and residence times from empirical flow calculations based on combustor volumes and modified to give favourable agreement with sampled concentrations at each condition. It should be emphasised that moderate uncertainty is associated with CRN modelling, and the CRN presented here was primarily used for qualitative analysis of trends found in the experimental results, rather than detailed prediction of untested conditions. Inlet temperatures always matched their equivalent experimental conditions. The reaction mechanism from Stagni et al. [39] with 31 chemical species and 203 reactions was selected as it showed good correlation with the

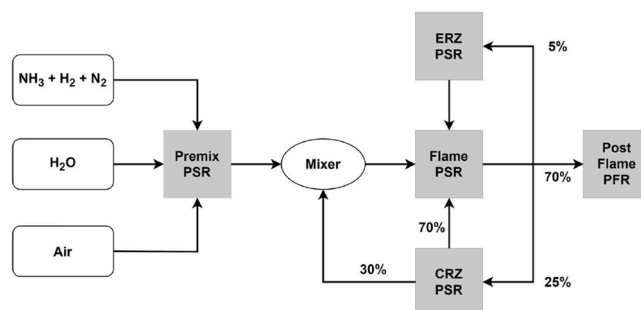


Fig. 2. Chemical reactor network (CRN).

experimental values in the present study, shown in the supplementary material Figs. S1, S2 and S4. It has also shown good performance in other recent studies [11,40,41].

3. Results and discussion

3.1. Comparison of 20 %_(vol.) cracked ammonia with 70/30 %_(vol.) NH₃/H₂

As discussed previously, 20 %_(vol.) cracked ammonia was chosen to compare the effects of adding the nitrogen from the cracking process into the fuel blend on emissions with a 70/30 %_(vol.) NH₃/H₂ blend. This is because it maintains a similar blend of NH₃/H₂ while preserving the required ratio of hydrogen to nitrogen.

Fig. 3 shows sampled emissions of 70/30 %_(vol.) NH₃/H₂ and 20 %_(vol.) cracked ammonia across a wide range of equivalence ratios and compares the two normalisation methodologies outlined in Section 2.2 to assess the impact on emissions from nitrogen dilution in the cracked ammonia case. Emissions of NO and NO₂ followed the expected unimodal trend, peaking at $\Phi = 0.9$ and 0.8, respectively. Both NO and NO₂ showed reduced emissions from the 20 %_(vol.) cracked ammonia flame from both normalisation methodologies. Fig. 3 also shows N₂O emissions were negligible for both cases at $\Phi > 0.8$, but below $\Phi = 0.8$, the 20 %_(vol.) cracked case showed a slight reduction in N₂O emissions. The emissions of unburned NH₃ showed the opposite relationship with equivalence ratio to the N₂O, instead showing negligible emissions below stoichiometry, and rapidly increasing at rich conditions. The cracked ammonia case emitted significantly more unburned ammonia than its equivalent ammonia/hydrogen blend. Fig. 3 also clearly demonstrates the narrower operating range for the 20 %_(vol.) cracked ammonia. Due to flame instabilities arising from reduced reactivity in the lean zone, no emission data could be captured below $\Phi = 0.7$, whereas the flame was still stable enough to capture emissions here for the 70/30 %_(vol.) case. However, the beginnings of flame instability can clearly be seen, with unburned NH₃ arising at $\Phi = 0.7$ for the 70/30 %_(vol.) case.

One reason for the reduction in NO emissions from the 20 %_(vol.) cracked flame shown in Fig. 3 relates to the flame morphology shown in Fig. 4. The 20 %_(vol.) cracked flame stabilised closer to the central axis of the burner, suggesting the NH or NH₂ radicals would be more likely to consume the NO produced there, as suggested from NO PLIF

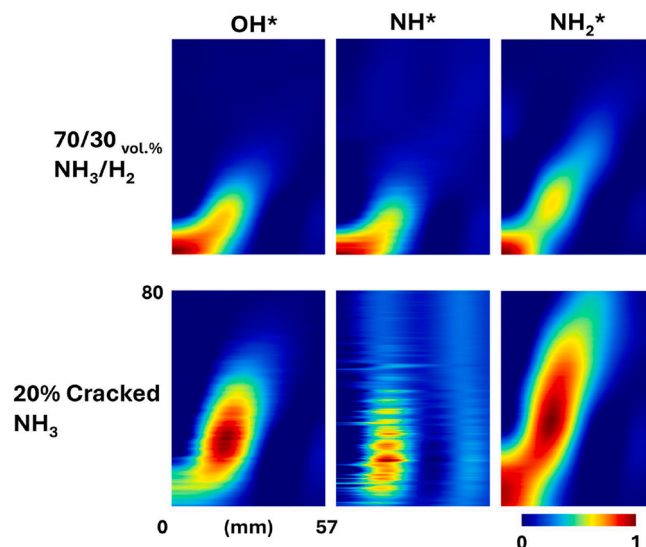


Fig. 4. Abel Transformed chemiluminescence (OH*, NH* and NH₂*) for 70/30 %_(vol.) NH₃/H₂ (top row) and 20 %_(vol.) cracked NH₃ (bottom row) at $\Phi = 0.8$. Colourmap of chemiluminescence images normalised to each image's maximum intensity.

measurements in [17], which used an identical burner geometry and flow rates as the 70/30 %_(vol.) case presented here. This centralisation of flame stabilisation may be a result of the nitrogen addition, which increased the burner inlet velocity by 2 % and Reynolds number by 2.5 % at $\Phi = 0.8$. The extra, relatively dense and inert nitrogen may have been captured in and disrupted the CRZ, preventing the flame from opening as much in the radial direction. Another reason for reduced NO emissions, particularly below stoichiometry, is related to flame temperature via NH and OH production. From the present CHEMKIN-PRO analysis, HNO is an intermediary chemical which can react with available H radicals to form NO, as shown in Eq. (1) and can be produced from the reaction in Eq. (2). These equations continuously appeared as significant in the present CRN study and have previously been identified as important in other studies using the same burner configuration [30] and different configurations [15,35].

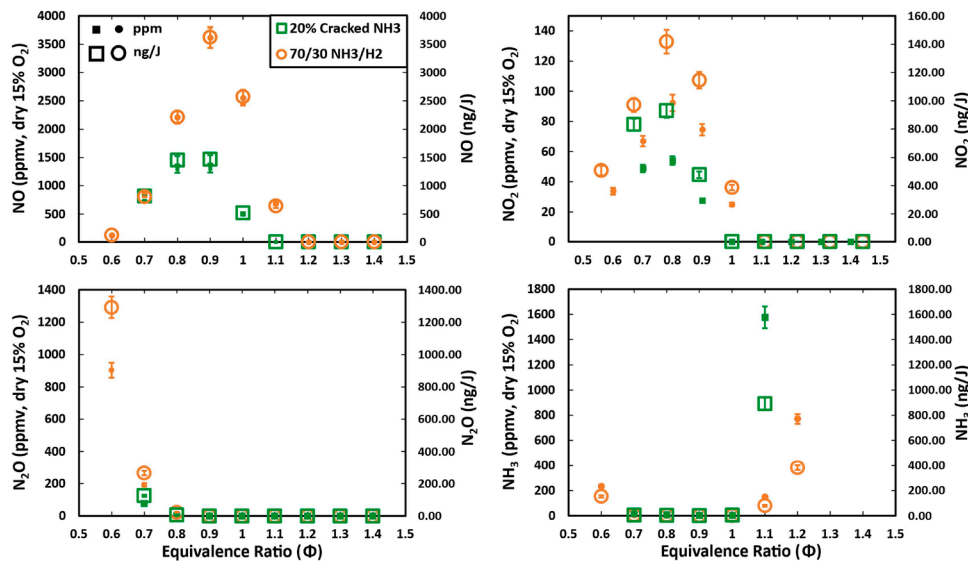


Fig. 3. Sampled emissions with changing equivalence ratio for 70/30 %_(vol.) NH₃/H₂ and 20 %_(vol.) cracked NH₃. NO (top left), NO₂ (top right), N₂O (bottom left) and unburned NH₃ (bottom right). Out of range NH₃ at rich conditions for both cases not plotted. Open and closed symbols refer to normalisation on a mass-power basis and a dry volumetric basis, respectively.

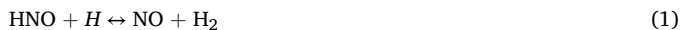


Fig. 4 shows the changes in radical formation between the two blends. Following previous studies [30] and discussed above in detail, the assumption of a positive correlation between ground state and emitting species was made for these three radicals. Although these images were normalised to their own maximum values, the images with poorer resolution and horizontal artefacts indicate lower signal intensity. The 20 %_(vol.) cracked ammonia case had lower OH* and NH* intensity as expected from the reduced measured post flame zone temperatures in Fig. 5. It should be noted that these temperature measurements proved less reliable at very rich conditions, likely due to flame length effects becoming significant. For example, at very rich conditions, the humidified flame was significantly longer and therefore closer to the thermocouple than the base condition flame. Although this was a relatively modest reduction of roughly 30 K at $\Phi = 1.1$, the added nitrogen would also consume more heat by raising the average specific heat capacity of the mixture, resulting in less heat being available for producing OH and NH for any given temperature. The reduction in reactivity from the presence of nitrogen would also reduce ammonia oxidation. Ultimately, HNO formation and consequently NO formation was reduced. This is in agreement with the study from Zhu et al. [42], which suggested OH* intensities could be a good marker for NO emissions in NH₃/H₂ flames.

Fig. 6 shows the NO rate of production (ROP) in the flame zone for the two cases, calculated in CHEMKIN-PRO using the CRN shown in Fig. 2. The NO dependence on NH and OH via HNO was validated in Fig. 6, which shows that when the NO consuming reaction of Eq. (3) was approximately equal for both cases, Eq. (1) was less than half for the 20 %_(vol.) cracked NH₃ case.



It should be noted that in Figs. 6 and 7, the 70/30 %_(vol.) NH₃/H₂ and 20 %_(vol.) cracked ammonia cases were each normalised by their own maximum ROPs to aid in visual comparison of the relative differences between reactions across both cases. The aim here was not to compare absolute values of ROP for each reaction, but to assess the differences in relative importance of each reaction between the two cases.

Fig. 4 also shows an increase in distribution of NH₂* intensity for the 20 %_(vol.) cracked NH₃ case, which would ordinarily reduce NO emissions from the consumption reactions of Eqs. (4) and (5). However, the rate of production analysis showed that for these two specific cases, at a

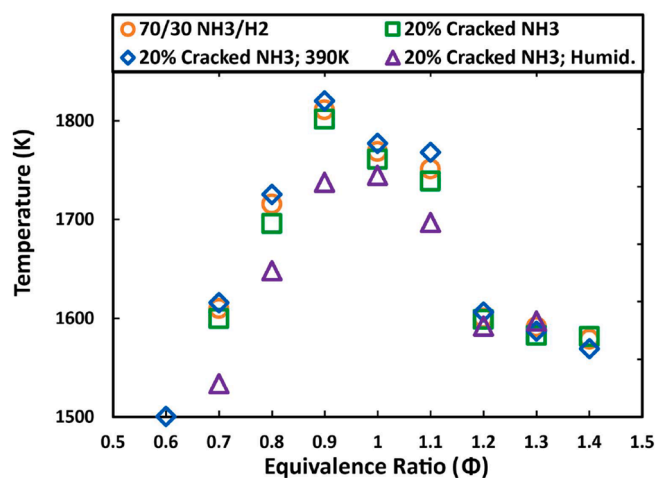


Fig. 5. Temperature captured by a thermocouple in the post-flame zone against equivalence ratio for each of the four cases considered. (Corrected for radiative and convective heat losses from the thermocouple).

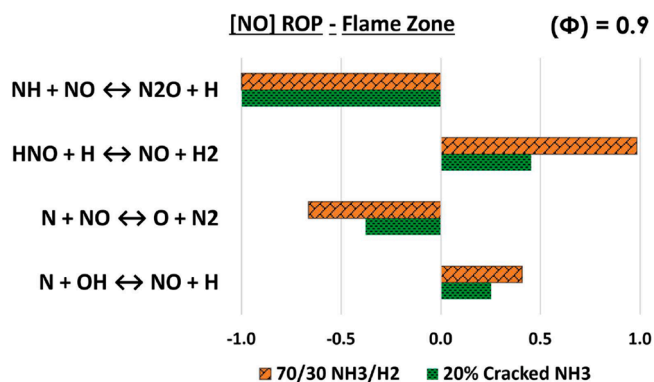


Fig. 6. Flame zone rate of production (ROP) for the most significant NO reactions for 70/30 %_(vol.) NH₃/H₂ (orange) and 20 %_(vol.) cracked NH₃ (green).

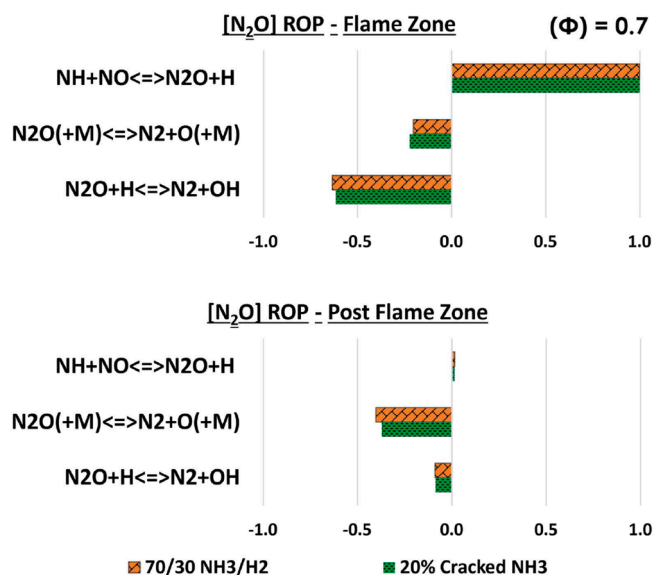
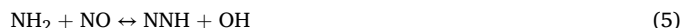


Fig. 7. Absolute and integrated ROPs of flame zone (top) and post flame zone (bottom) for the most significant N₂O reactions for 70/30 %_(vol.) NH₃/H₂ (orange) and 20 %_(vol.) cracked NH₃ (green).

lean equivalence ratio of $\Phi = 0.9$ where NH₂* intensity was relatively low, these reactions were not significant, unlike at rich conditions. Instead, at slightly lean conditions, NH and atomic nitrogen were mainly responsible for NO consumption.



It is also important to note that the equivalence ratio at which negligible measured NO was reached reduced from $\Phi = 1.2$ to $\Phi = 1.1$. Also shown in Fig. 3, the peak of 142 ng/J of NO₂ was found at $\Phi = 0.8$ for the 70/30 %_(vol.) NH₃/H₂ case and was roughly 50 % larger than the peak value in the 20 %_(vol.) cracked NH₃ case. This demonstrates a similar relationship between the cases for NO₂ and NO, but with a smaller difference.

The N₂O reduction shown for the 20 %_(vol.) cracked case in Fig. 3 is also related to flame morphology. On a temperature basis, the addition of N₂ into the fuel slightly reduces the reactivity and hence flame speed, elongating the flame as shown in Fig. 3. Fig. 7 shows the N₂O ROP in both the flame zone and post-flame zone for the two cases, calculated using the CRN shown in Fig. 2. It shows that in the flame zone, consumption of N₂O by Eq. (7) was 11 % higher for the 20 %_(vol.) cracked

ammonia case, over the 70/30_(vol.) NH₃/H₂ case. This compounds with the longer 20 %_(vol.) cracked flame providing the increase in residence time that Eq. (7) requires [30], as well as a larger flame volume to act in. There was a 3 % reduction in consumption of N₂O via Eq. (6) for the 20 %_(vol.) cracked ammonia case, which was expected as the required free H atom availability for that reaction is temperature dependent, and the cracked ammonia case had a cooler temperature, shown in Fig. 5. Fig. 7 also showed that although consumption of N₂O was slightly lower in the post flame zone for the 20 %_(vol.) cracked NH₃ case, it was not enough to offset the increase in consumption found in the flame zone.



The same mechanism affected emissions of unburned NH₃, with the 20 %_(vol.) cracked case producing a roughly 600 % increase in NH₃ slip over the 70/30 %_(vol.) NH₃/H₂ blend at $\Phi = 1.1$. This alone demonstrates the reduction in measured NO_x emissions is not solely the result of diluting the exhaust gas sample with the added nitrogen, as that would have also reduced NH₃ emissions. The right-hand axis in Fig. 3 confirms this, showing on a mass/power basis, nitrogen dilution had a relatively small effect on emissions and all trends were maintained across both methodologies. This was to be expected considering the small amount of nitrogen injected – just 2.3 % of the total inlet mass flow at stoichiometry. When further increasing the equivalence ratio above $\Phi = 1.1$, the unburned NH₃ values for both blends were higher than the gas analyser limit and are therefore not present on this plot.

These findings of reduced NO and NO₂ but increased NH₃ emissions indicate that using 20 %_(vol.) cracked ammonia as a fuel in a single stage burner would have to be at an equivalence ratio of less than 1.1, at which point NO emissions become an issue again. Therefore, a potential NO mitigation strategy of humidification was investigated in more detail.

3.2. Effect of varying inlet temperature and humidification on 20 %_(vol.) cracked NH₃

In this section, only the 20 %_(vol.) cracked NH₃ case was examined. First, inlet temperatures were increased from 295 K to 390 K. Then, steam injection was investigated, with a volumetric H₂O fraction in the fuel of 30 % whilst maintaining the higher inlet temperature of 390 K. The inlet temperature was maintained at 390 K for the humidification case so that the steam generated within the burner head would not

condense back into liquid water upon injection into the premixing chamber. As a result, the quenching effect of water vaporisation within the flame would be minimal due to effective experimental design – only steam is injected into the flame, with no water droplet transport. Furthermore, wall cooling of the face plate due to waste heat being used to vaporise water into steam was accounted for in the CRN with changes in simulated heat loss.

Fig. 8 shows the emissions results from these three cases. As in Section 3.1, the NO and NO₂ emissions from each case followed the same unimodal shape, peaking around $\Phi = 0.9$ and $\Phi = 0.8$, respectively. NO and NO₂ also have the same trend, with the emissions increasing with increased inlet temperature, and then reducing with the injection of steam, compared to the base case of 20 %_(vol.) cracked NH₃ at 295 K inlet temperature. All three cases reached negligible NO emissions at $\Phi = 1.1$. N₂O emissions were all negligible at and above $\Phi = 0.8$, apart from for the humidified case, which additionally proved significantly higher than the other two cases at $\Phi = 0.7$. Here, the case with increased inlet temperature emitted half of the N₂O. For all cases, both unburned fuels were undetectable at and below stoichiometry, but began to rapidly increase above $\Phi = 1$. The NH₃ emissions for the humidified case were notably high, and all three cases were above the gas analyser's dilution range already at $\Phi = 1.2$ and are therefore not present in Fig. 8. This was likely due to decreased reactivity as discussed in Section 3.1.

Interestingly, trends inverted between unburned NH₃ and H₂. For NH₃, humidification resulted in higher emissions than the base case and increased inlet temperatures resulted in lower emissions. The opposite was true for emissions of unburned H₂, but these results are likely related. The approximately 50 K lower temperature post-flame zone measured in Fig. 5 for the humidified case at $\Phi = 1.1$ could result in less of the unburned NH₃ being thermally cracked into H₂ and N₂ in the absence of oxygen in the exhaust. This would result in higher unburned NH₃ and lower unburned H₂ than the base case, as shown in Fig. 8. Above $\Phi = 1.3$, unburned H₂ emissions began to reduce, which could also be related to generally lower post flame zone temperatures cracking less NH₃ into H₂ and N₂, regardless of injection temperature or humidification. Fig. 8 also demonstrates an increase in flame stability when the inlet temperature was increased to 390 K, with emissions stable enough to measure at $\Phi = 0.6$. At this same equivalence ratio in Fig. 3, unburned NH₃ emissions were significant, demonstrating the flame instability. However, the 20 %_(vol.) cracked NH₃ case at an inlet temperature of 390 K had comparatively far lower NH₃ emissions, suggesting that the reduction in stable operating range from the nitrogen present in cracked

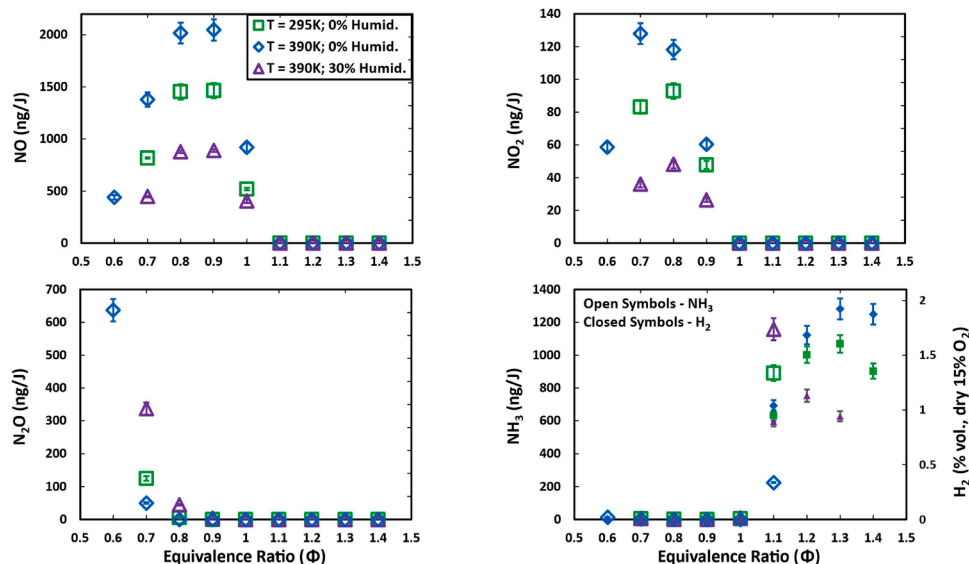


Fig. 8. Sampled emissions with changing equivalence ratio for 20 %_(vol.) cracked NH₃ at ambient and increased inlet temperature and with humidification. NO (top left), NO₂ (top right), N₂O (bottom left) and unburned NH₃ and H₂ (bottom right). Out of range NH₃ at rich conditions not plotted for all three cases.

ammonia flames was compensated by an increase in inlet temperature of just 100 K.

To reduce graph complexity, emissions are presented only on a mass/power basis in Fig. 8 as it provides a more representative comparison than a dry volumetric basis by accounting for both nitrogen and steam dilution in the exhaust gases for all emissions apart from H₂. In order to calculate non-zero emissions on a mass/power basis, the concentration of all exhaust gases must be known. As unburned NH₃ was not measurable above $\Phi = 1.1$, H₂ emissions could not be calculated in ng/J, so are presented here as dry, 15 % O₂ volumetric percentage.

However, at $\Phi = 1.1$, both unburned NH₃ and H₂ were measurable at the same time. To check whether steam dilution influenced emissions results here, the H₂ emissions were calculated on a mass/power basis. Fig. 9 below shows NH₃ and H₂ emissions at $\Phi = 1.1$, as well as calculated combustion efficiency for each of the three cases from Eq. (8). It shows the same inversion of trends as shown for 15 % O₂, dry, proving that dilution from H₂O (discussed in detail in Section 2.2) did not change the trends shown in Fig. 8. These H₂ values also emphasise that although ~1 % emission of H₂ appears exceptionally high, they can be explained by hydrogen's low density, and on a mass/power basis, emissions of H₂ are similar to those of unburned NH₃. Fig. 9 also shows that despite the inversion of trends of emissions of NH₃ and H₂, the combustion efficiency follows the expected trend of elevated inlet temperature having higher efficiency, and humidification having lower efficiency than the base 20 % (vol.) cracked case. None of the cases emitted detectable amounts of unburned fuel at $\Phi < 1.1$, resulting in combustion efficiencies of 100 %. All cases produced too high emissions of unburned NH₃ to measure at $\Phi > 1.1$, so combustion efficiency could not be calculated.

$$\eta = 1 - \frac{\dot{m}(NH_3 + H_2)_{out}}{\dot{m}(NH_3 + H_2)_{in}} \quad (8)$$

Fig. 10 shows the intensity and spatial variations of OH*, NH* and NH₂* from the three cases at $\Phi = 0.9$. Each set of OH*, NH* and NH₂* images was normalised to the maximum intensity found for each species across all three cases. Here, that was found in the T = 390 K; 0 % Humid. case. This methodology is useful as it allows the variations in intensity to be compared qualitatively, while simultaneously maintaining enough information within each image to identify any spatial differences. If the images were not normalised to each species' maximum intensity, no correlations with the ROP calculations could be drawn. Fig. 11 shows the variations in rate of production and consumption of NO in the flame zone for the three cases, also at $\Phi = 0.9$. Here, the reason for the increase in NO when inlet temperature was increased to 390 K and the significant reduction for the humidified case can be explained, as OH* and NH* followed the same trend as NO for these cases in Fig. 8. Again, from Eq. (2), an increase in NH and OH promotes HNO formation which ultimately forms NO, as demonstrated for the 390 K case in Fig. 11. This is

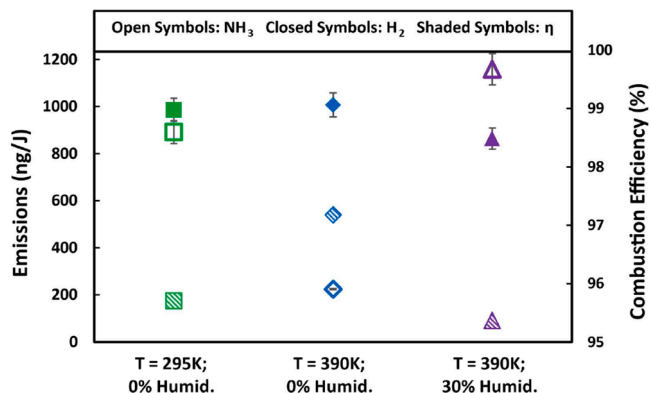


Fig. 9. Sampled emissions of unburned NH₃ and H₂, and resulting combustion efficiency at $\Phi = 1.1$ for each case.

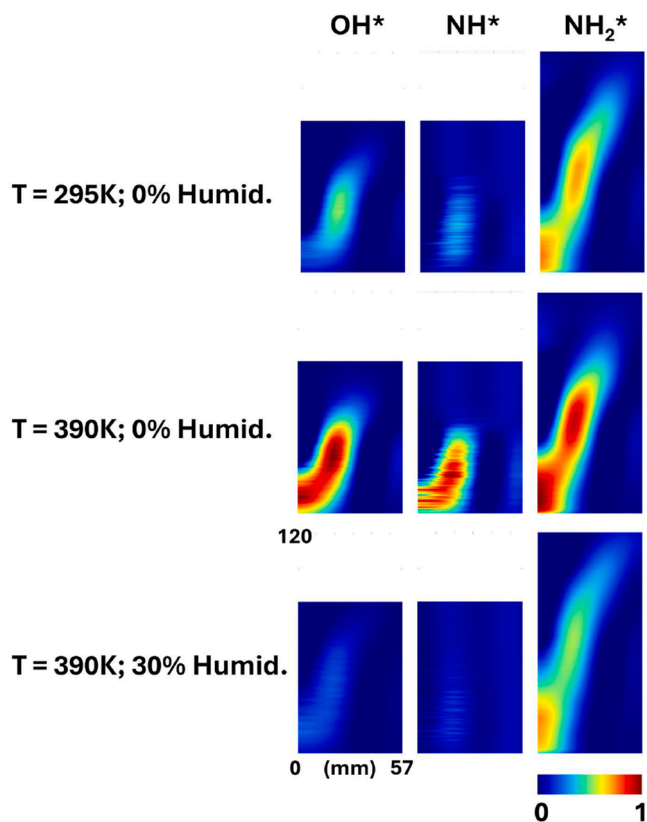


Fig. 10. Abel Transformed chemiluminescence (OH*, NH* and NH₂*) for 20 % (vol.) cracked NH₃ at ambient (top row), increased inlet temperature (middle row) and with humidification (bottom row) at $\Phi = 0.9$. Colourmap of chemiluminescence images normalised to the species dataset maximum.

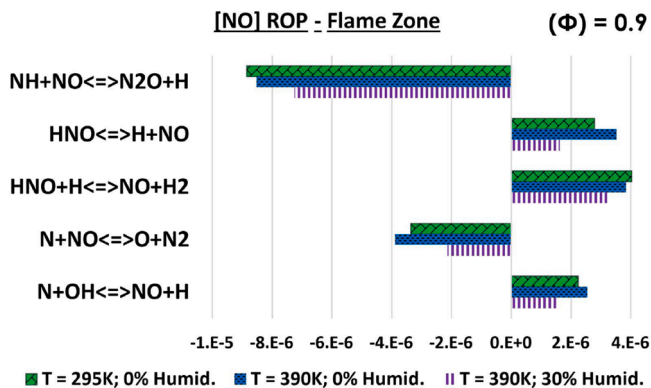


Fig. 11. Flame zone rate of production (ROP) [Unit – mole/cm³-sec] for the most significant NO reactions for 20 % (vol.) cracked NH₃ at ambient and increased inlet temperatures, and with humidification.

further validated by Eq. (9), which consumes OH and rose for the 390 K case and decreased for the humidified case in Fig. 11.



The significant reduction in NO this caused for the humidification case should be highlighted, as the peak NO was measured as below 900 ng/J. As in Section 3.1, the “de-NOxing” [43] effect of NO reduction from NH₂ in the reactions in Eqs. (4) and (5) were found to be not particularly significant at the lean condition ($\Phi = 0.9$) considered here, with an increase in inlet temperature, nor with humidification and are therefore not shown in Fig. 11. This was expected due to the relative lack

of NH_2 intensity at lean conditions, compared to rich.

Interestingly, humidification was even more effective at reducing NO_2 emissions than NO emissions. While the NO emissions were reduced by 40 %, the NO_2 emissions were halved. An in-depth ROP analysis to determine the reasoning behind this enhanced reduction in NO_2 emission was not possible due to the employed kinetic reaction mechanism not accurately capturing NO_2 concentrations, shown in Supplementary Material Fig. S3. However, it is hypothesised that the reaction in Eq. (10) could have played a role as increased concentration of H_2O from steam injection might have provided more free O atoms to consume NO_2 .



The sub-optimal mechanism performance in predicting NO_2 concentrations has been noted in the literature previously [11], with it being suggested that the mechanisms may not accurately account for ammonia's high third body efficiency enhancing the conversion of NO into NO_2 , through the reaction shown in Eq. (11).



In Fig. 8, N_2O halved for the $T = 390$ K case and more than doubled for the humidified case – relative to the base 20 %_(vol.) cracked ammonia case – and can be explained by considering the flame length and free H radical availability. Fig. 12 shows the differences in intensity weighted centroid of captured OH^* at two different equivalence ratios for each of the cases. Together with Fig. 8, they qualitatively and quantitatively demonstrate that for both equivalence ratios, the flame shortened with an increase in inlet temperature and lengthened with humidification, in line with the temperatures shown in Fig. 5. Fig. 12 also shows the humidified flames were narrower radially, stabilising closer to the central axis of the burner. Furthermore, it shows the significant difference in flame length between $\Phi = 0.7$ and $\Phi = 0.9$ for all three cases, suggesting equivalence ratio played a larger role in varying the flame morphology than humidification did. The significant difference in flame length between the two equivalence ratios could also explain the larger differences between cases at $\Phi = 0.9$ compared to $\Phi = 0.7$. OH^* chemiluminescence was selected for comparing the intensity weighted centroid locations instead of NH_2^* due to $\Phi = 0.7$ being presented. As discussed in Section 2.3, at very lean conditions, the influence of NO_2^* in the visible spectrum may become significant when compared to NH_2^* . However, the same trends in centroid variations across conditions shown in Fig. 12 for OH^* were also found for NH^* and NH_2^* centroids.

Fig. 13 shows the rate of production and consumption of N_2O in both the flame zone and post-flame zone, calculated using the CRN in Fig. 2 for all three cases. N_2O was mostly produced in the flame zone, shown

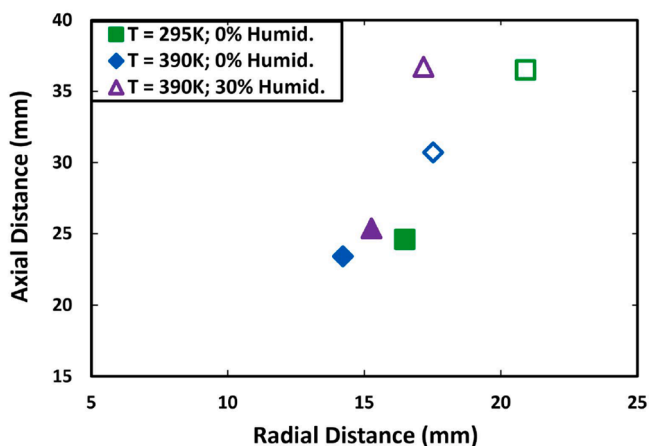


Fig. 12. Intensity weighted centroid locations of Abel transformed OH^* chemiluminescence images at $\Phi = 0.9$ (empty symbols) and $\Phi = 0.7$ (filled symbols).

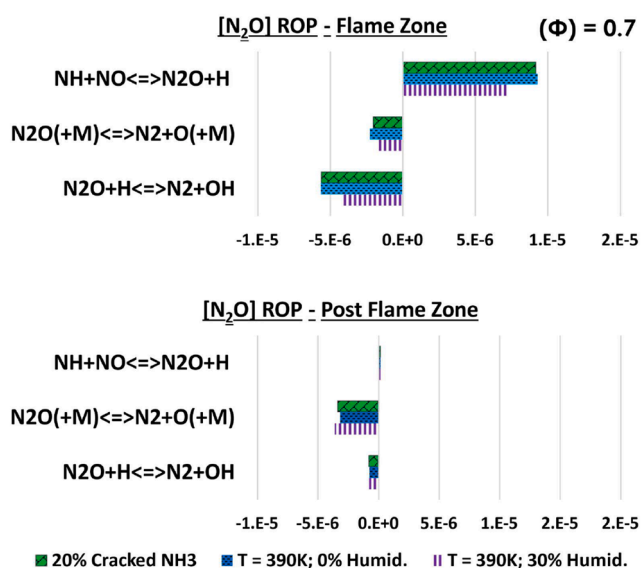


Fig. 13. Absolute and integrated ROPs of flame zone (top [Unit – mole/ cm^3 -sec]) and post flame zone (bottom [Unit – mole/ cm^2 -sec]) for the most significant N_2O reactions for 20 %_(vol.) cracked NH_3 at ambient and increased inlet temperatures, and with humidification.

by Eq. (3) in Fig. 13. In the post flame zone, the effect of the third body reaction (Eq. (7)), requiring a longer residence time [30] is evident. As the humidified flame was longer, the required residence time was met and so more N_2O could be consumed. Conversely, the higher temperature, shortened flame of the 20 %_(vol.) cracked NH_3 at 390 K inlet temperature showed less consumption from the third body reaction equation. In the flame zone it appears that the reverse trend is followed, but the units of the ROP (mole/ cm^3 -sec) must again be considered. As the humidified flame is longer, it must also have a larger flame volume and residence time. Therefore, this apparently lower ROP is likely to result in more N_2O being consumed as the ROP has a larger volume and longer time to act in. Ultimately, the largest consuming reaction was found to be in the flame zone, with Eq. (6). The free hydrogen atom requirement for this reaction has a high temperature requirement, demonstrated with the lowest temperature humidified case having the lowest negative ROP.

To validate the chemiluminescence images and to concisely show how spectral signatures vary with equivalence ratio, the chemiluminescence emission from the flame was recorded using an optical spectrometer, shown in Fig. 14. Fig. 14 follows the same trend as the chemiluminescence images in Fig. 10, in that the 390 K inlet temperature case had the highest intensity, followed by the 295 K case and with the humidified case having the lowest. The OH^* and NH^* intensities follow the same unimodal curve with the peak between $\Phi = 0.8$ – 1.0 as the NO emission curve in Fig. 8, suggesting they could be used as a rough analogue for NO emissions if a relatively low-cost spectrometer is the only diagnostic tool available. It also again evidences the role OH and NH have in NO production via the HNO reactions. From a practical perspective, the slight variation in peaks of OH^* and NH^* between the three cases is worth highlighting. For the base 20 %_(vol.) cracked ammonia case, OH^* and NH^* peaked at $\Phi = 0.9$ and 1.0 , respectively. However, for the two other cases of elevated temperature and 30 % humidification, both chemiluminescence peaks were shifted leaner, to $\Phi = 0.8$ and 0.9 . NH_2^* rose sharply above $\Phi = 1.0$ for all three cases, at which point the NH_2 reactions' (Eqs. (4) and (5)) role in NO consumption more than doubled. The previously mentioned shift in peak chemiluminescent intensity found for OH^* and NH^* was not found for NH_2^* , as all three cases peaked at $\Phi = 1.2$.

Fig. 8 shows a decrease in NO emissions in very lean conditions, seemingly suggesting viability for low emission cracked NH_3 flames.

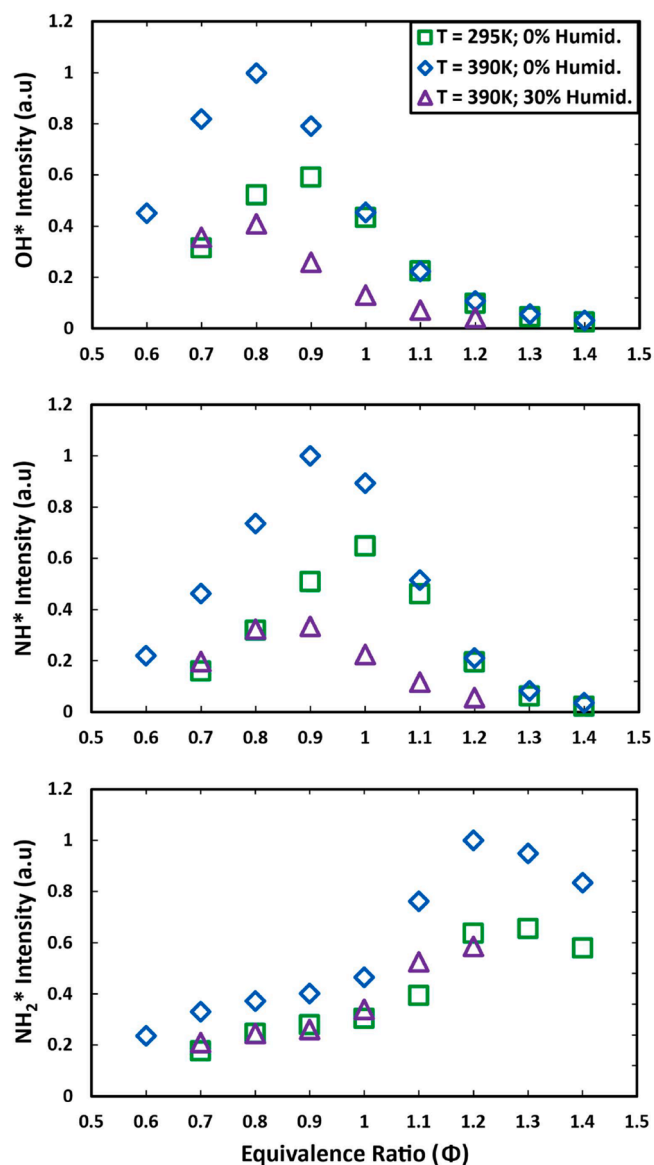


Fig. 14. Normalised optical spectrometry results for OH*, NH* and NH₂* chemiluminescence against equivalence ratio for 20 %_(vol.) cracked NH₃ at ambient and increased inlet temperatures, and with humidification.

However, there is also an increase in N₂O emissions. Insulating refractory material found in gas turbines, boilers and furnaces would likely reduce heat loss in higher power flames, leading to higher temperatures in both the flame and post flame zones. From Eq. (6), N₂O emissions might be reduced further with reduced heat loss [44]. Unfortunately, higher temperatures reducing N₂O would be offset by producing more NO from the HNO reactions discussed previously across Sections 3.1 and 3.2. This highlights the necessity of operating ammonia flames at more rich conditions to reduce emissions of NO, NO₂ and N₂O to negligible quantities simultaneously, as the present work has demonstrated, with possible operation at a leaner equivalence ratio ($\Phi = 1.1$) than previously found. Although humidification was also shown to reduce H₂ emissions, to reduce unburned NH₃ emissions concurrently, the mechanisms which cause instabilities at the slightly rich condition need to be understood and controlled in a future study. Humidification appears to complement other methodologies for reducing NO emissions such as axial staging and needs to be investigated concurrently.

4. Conclusions

In this study, the emissions performance from a 70/30 %_(vol.) NH₃/H₂ blend was experimentally and numerically compared with a 20 %_(vol.) cracked NH₃ blend. The 20 %_(vol.) cracked NH₃ had 50 % lower peak NO_x emissions mainly due to changes in flame morphology and temperature, but increased unburned NH₃ slip, as well as narrower stability regions due to a reduction in reactivity.

The 20 %_(vol.) cracked NH₃ blend was then investigated more thoroughly by examining the effects of increased inlet temperature and 30 %_(vol.) fuel humidification. With an increase in inlet temperature, NO and NO₂ increased due to thermal NO_x production and an increase in OH and NH forming HNO. However, stability limits were widened and N₂O emissions decreased due to the enhancement of H radical production breaking down N₂O to N₂.

With humidification, peak NO and NO₂ emissions decreased by 40 % and 48 %, respectively, mainly due to a reduced production of OH and NH. Little difference between cases was found in NO consumption by NH₂ here at $\Phi = 0.9$ as NH₂* intensity was relatively low.

Humidification also caused N₂O emission to more than double at the very lean condition due to a reduction in the availability of free H radicals from lower flame temperatures, despite a longer flame enabling the third body reaction to consume more N₂O. Unburned NH₃ emission was higher at rich humidified conditions due to reduced reactivity which resulted in flame instabilities. Unburned H₂ emission was reduced, likely resulting from reduced temperatures in the exhaust thermally cracking less of the unburned NH₃ into H₂ and N₂.

Novelty and significance statement

The novelty of this research is the first examination of the emissions from humidified cracked ammonia flames, which are significantly more practical to industry than ammonia/hydrogen flames. Beyond this, it differs from previous works on humidified ammonia/hydrogen flames in the literature by measuring NO, NO₂, N₂O, NH₃ and H₂ emissions simultaneously and corrects for the volumetric dilution effect of the steam in the exhaust gas for the first time. Furthermore, it demonstrates a more industrially applicable burner design where steam was generated by utilising waste heat from the burner, rather than by using a separate electrical heating system. It is significant because it demonstrates a method to achieve negligible NO_x and carbon emissions from a more practical fuel, at leaner equivalence ratios than previously found.

CRediT authorship contribution statement

Jordan Davies: Writing – original draft, Visualization, Methodology, Investigation, Data curation. **Syed Mashruk:** Writing – review & editing, Supervision, Methodology, Investigation, Data curation. **Daisuke Sato:** Investigation. **Luca Mazzotta:** Investigation. **Daniel Pugh:** Writing – review & editing, Supervision. **Agustin Valera-Medina:** Writing – review & editing, Supervision.

Declaration of competing interest

The authors declare that they have no known competing financial interests or personal relationships that could have appeared to influence the work reported in this paper.

Acknowledgements

This work was supported by the AMBURN project with funding from the Department for Energy Security and Net Zero (DESNZ) (Grant Number: IFS2-06-FLO), the EPSRC Centre for Doctoral Training in Resilient Decarbonised Fuel Energy Systems (Grant Number: EP/S022996/1) and Reaction Engines Ltd. The research was undertaken at Cardiff University's Thermofluids Lab (W/0.17) with invaluable

technical support from Mr. Malcolm Seaborne.

Supplementary materials

Supplementary material associated with this article can be found, in the online version, at [doi:10.1016/j.combustflame.2025.113984](https://doi.org/10.1016/j.combustflame.2025.113984).

References

- [1] A. Valera-Medina, F. Amer-Hatem, A.K. Azad, I.C. Dedoussi, M. De Joannon, R. X. Fernandes, et al., Review on ammonia as a potential fuel: from synthesis to economics, *Energy Fuels* 35 (2021) 6964–7029.
- [2] A. Valera-Medina, H. Xiao, M. Owen-Jones, W.I.F. David, P.J. Bowen, Ammonia for power, *Prog. Energ. Combust.* 69 (2018) 63–102.
- [3] L. Kang, W. Pan, J. Zhang, W. Wang, C. Tang, A review on ammonia blends combustion for industrial applications, *Fuel* 332 (2023) 126150.
- [4] W.S. Chai, Y. Bao, P. Jin, G. Tang, L. Zhou, A review on ammonia, ammonia-hydrogen and ammonia-methane fuels, *Renew. Sust. Energ. Rev.* 147 (2021) 111254.
- [5] A.M. Elbaz, S. Wang, T.F. Guiberti, W.L. Roberts, Review on the recent advances on ammonia combustion from the fundamentals to the applications, *Fuel Commun* 10 (2022) 100053.
- [6] S. Mashruk, M.O. Viguera-Zuniga, M.E. Tejada-del-Cueto, H. Xiao, C. Yu, U. Maas, et al., Combustion features of CH₄/NH₃/H₂ ternary blends, *Int. J. Hydrogen Energy* 47 (2022) 30315–30327.
- [7] A.A. Khateeb, T.F. Guiberti, X. Zhu, M. Younes, A. Jamal, W.L. Roberts, Stability limits and NO emissions of technically-premixed ammonia-hydrogen-nitrogen-air swirl flames, *Int. J. Hydrogen Energy* 45 (2020) 22008–22018.
- [8] S. Mukherjee, S.V. Devaguptapu, A. Sviripa, C.R.F. Lund, G. Wu, Low-temperature ammonia decomposition catalysts for hydrogen generation, *Appl. Catal. B-Environ.* 226 (2018) 162–181.
- [9] M. Asif, S. Sidra Bibi, S. Ahmed, M. Irshad, M. Shakir Hussain, H. Zeb, et al., Recent advances in green hydrogen production, storage and commercial-scale use via catalytic ammonia cracking, *Chem. Eng. J.* 473 (2023) 145381.
- [10] A. Hayakawa, Y. Arakawa, R. Mimoto, K. Somarathne, T. Kudo, H. Kobayashi, Experimental investigation of stabilization and emission characteristics of ammonia/air premixed flames in a swirl combustor, *Int. J. Hydrogen Energy* 42 (2017) 14010–14018.
- [11] S. Mashruk, M. Kovaleva, A. Alnasif, C.T. Chong, A. Hayakawa, E.C. Okafor, et al., Nitrogen oxide emissions analyses in ammonia/hydrogen/air premixed swirling flames, *Energy* 260 (2022) 125183.
- [12] D. Pugh, P. Bowen, A. Valera-Medina, A. Giles, J. Runyon, R. Marsh, Influence of steam addition and elevated ambient conditions on NO_x reduction in a staged premixed swirling NH₃/H₂ flame, *Proc. Combust. Inst.* 37 (2019) 5401–5409.
- [13] D. Pugh, P. Bowen, B. Goktepe, A. Giles, S. Mashruk, A. Valera-Medina, et al., Influence of steam and elevated ambient conditions on N₂O in a premixed swirling NH₃/H₂ flame, in: *Proceedings of the ASME Turbo Expo, 2023*, pp. 3A–2023.
- [14] A.A. Khateeb, T.F. Guiberti, G. Wang, W.R. Boyette, M. Younes, A. Jamal, et al., Stability limits and NO emissions of premixed swirl ammonia-air flames enriched with hydrogen or methane at elevated pressures, *Int. J. Hydrogen Energy* 46 (2021) 11969–11981.
- [15] M. Ditaranto, I. Saanum, Experimental study on the effect of pressure on single and two stage combustion of decomposed ammonia (NH₃ H₂ N₂) blends over a swirl stabilized burner, *Combust. Flame* 262 (2024) 113368.
- [16] D. Pugh, A. Valera-Medina, P. Bowen, A. Giles, B. Goktepe, J. Runyon, et al., Emissions performance of staged premixed and diffusion combustor concepts for an NH₃ air flame with and without reactant humidification, *J. Eng. Gas Turbine Power* 143 (2021).
- [17] S. Mashruk, A. Alnasif, C. Yu, J. Thatcher, J. Rudman, L. Peronski, et al., Combustion characteristics of a novel ammonia combustor equipped with stratified injection for low emissions, *Journal of Ammonia Energy* 1 (2023).
- [18] E.D. Larson, R.H. Williams, Steam-injected gas turbines, *J. Eng. Gas Turbine Power* 109 (1987) 55–63.
- [19] K. Nishida, T. Takagi, S. Kinoshita, Regenerative steam-injection gas-turbine systems, *Appl. Energy* 81 (2005) 231–246.
- [20] C. Wei, S. Zang, Experimental investigation on the off-design performance of a small-sized humid air turbine cycle, *Appl. Therm. Eng.* (2013) 166–176.
- [21] F. Reale, R. Sannino, Water and steam injection in micro gas turbine supplied by hydrogen enriched fuels: numerical investigation and performance analysis, *Int. J. Hydrogen Energy* 46 (2021) 24366–24381.
- [22] M. Gutesa Božo, M.O. Viguera-Zuniga, M. Buffi, T. Seljak, A. Valera-Medina, Fuel rich ammonia-hydrogen injection for humidified gas turbines, *Appl. Energy* 251 (2019) 113334.
- [23] M. Hayashi, A. Hayakawa, T. Kudo, H. Kobayashi, Effects of water vapor dilution on the laminar burning velocity and markstein length of ammonia/water vapor/air premixed laminar flames, *Energy and Fuels* 36 (2022) 12341–12349.
- [24] A. Valera-Medina, M.O. Viguera-Zuniga, H. Shi, S. Mashruk, M. Alnajideen, A. Alnasif, et al., Ammonia combustion in furnaces: a review, *Int J Hydrogen Energy* 49 (2024) 1597–1618.
- [25] P. Berwal, S. Kumar, B. Khandelwal, A comprehensive review on synthesis, chemical kinetics, and practical application of ammonia as future fuel for combustion, *Journal of the Energy Institute* 99 (2021) 273–298.
- [26] R.B. Teel, Stress-corrosion cracking of steels in ammonia with consideration given to OTEC design: a survey, Report No. ANL/OTEC-BCM-008, Argonne National Laboratory, Argonne, IL, USA, 1980.
- [27] M. Kovaleva, D. Dziedzic, S. Mashruk, S. Evans, A. Valera-Medina, E. Galindo-Nava, The Evaluation of Ammonia/Hydrogen Combustion on the H Permeation and Embrittlement of Nickel-Base Superalloys, *ASME Turbo Expo, 2022 paper GT2022-82239*.
- [28] D. Wang, M.A. Ali, K. Sharma, S.F. Almojil, A. Alizadeh, A.F. Alali, et al., Multiphase numerical simulation of exergy loss and thermo-hydraulic behaviour with environmental considerations of a hybrid nanofluid in a shell-and-tube heat exchanger with twisted tape, *Eng Anal Bound Elem* 147 (2023) 1–10.
- [29] K. Chen, D. Seo, P. Canteenwalla, The effect of high-temperature water vapour on degradation and failure of hot section components of gas turbine engines, *Coatings* 11 (2021) 1061.
- [30] S. Mashruk, E.C. Okafor, M. Kovaleva, A. Alnasif, D. Pugh, A. Hayakawa, et al., Evolution of N₂O production at lean combustion condition in NH₃/H₂/air premixed swirling flames, *Combust. Flame* 244 (2022) 112299.
- [31] British Standards Institute, British Standard ISO 11042-1:1996, Gas turbines, Exhaust Gas Emission Measurement and Evaluation, UK, 1996.
- [32] C.M. Douglas, S.L. Shaw, T.D. Martz, R.C. Steele, D.R. Noble, B.L. Emerson, et al., Pollutant emissions reporting and performance considerations for hydrogen-hydrocarbon fuels in gas turbines, *J. Eng. Gas Turbine Power* 144 (2022).
- [33] S. Mashruk, Nitric oxide formation analysis using chemical reactor modelling and laser induced fluorescence measurements on industrial swirl flames, Cardiff University, 2020.
- [34] S.B. Nourani Najafi, A.V. Mokhov, H.B. Levinsky, Investigation of the stability, radiation, and structure of laminar coflow diffusion flames of CH₄/NH₃ mixtures, *Combust. Flame* 244 (2022) 112282.
- [35] A. Hayakawa, T. Goto, R. Mimoto, T. Kudo, H. Kobayashi, NO formation/reduction mechanisms of ammonia/air premixed flames at various equivalence ratios and pressures, *Mech. Eng. J.* 2 (2015) 14–00402.
- [36] A.A. Konnov, An exploratory modelling study of chemiluminescence in ammonia-fuelled flames, Part 1, *Combust. Flame* 253 (2023) 112788.
- [37] W. Weng, M. Aldén, Z. Li, Visible chemiluminescence of ammonia premixed flames and its application for flame diagnostics, *Proc. Comb. Inst.* 39 (2023) 4327–4334.
- [38] S. Mashruk, H. Xiao, D. Pugh, M.C. Chiong, J. Runyon, B. Goktepe, et al., Numerical analysis on the evolution of NH₂ in ammonia/hydrogen swirling flames and detailed sensitivity analysis under elevated conditions, *Combust. Sci. Technol.* 195 (2023) 1251–1278.
- [39] A. Stagni, C. Cavallotti, S. Arunthanayothin, Y. Song, O. Herbinet, F. Battin-Leclerc, et al., An experimental, theoretical and kinetic-modeling study of the gas-phase oxidation of ammonia, *React. Chem. Eng.* 5 (2020) 696–711.
- [40] A. Hayakawa, M. Hayashi, M. Kovaleva, G.J. Gotama, E.C. Okafor, S. Colson, et al., Experimental and numerical study of product gas and N₂O emission characteristics of ammonia/hydrogen/air premixed laminar flames stabilized in a stagnation flow, *Proc. Comb. Inst.* 39 (2023) 1625–1633.
- [41] S.E. Zitouni, S. Mashruk, N. Mukundakumar, P. Brequigny, A. Zayoud, E. Pucci, et al., Ammonia Blended fuels—energy solutions for a green future, in: 10th International Gas Turbine Conference, 2021 paper IGTC21-62.
- [42] X. Zhu, A.A. Khateeb, T.F. Guiberti, W.L. Roberts, NO and OH* emission characteristics of very-lean to stoichiometric ammonia–hydrogen–air swirl flames, *Proc. Comb. Inst.* 38 (2021) 5155–5162.
- [43] P. Glarborg, J.A. Miller, B. Ruscic, S.J. Klippenstein, Modeling nitrogen chemistry in combustion, *Prog. Energ. Combust.* 67 (2018) 31–68.
- [44] E.C. Okafor, M. Tsukamoto, A. Hayakawa, K.A. Somarathne, T. Kudo, T. Tsujimura, et al., Influence of wall heat loss on the emission characteristics of premixed ammonia-air swirling flames interacting with the combustor wall, *Proc. Combust. Inst.* 38 (2021) 5139–5146.